Journal of Sustainable Development of Natural Resources Management

http://www.sdewes.org/jsdnarema

Year 2026, Volume 2, Issue 3, 1010772

Original Research Article

Design and Implementation of a Buck DC/DC Converter Battery Charger for a PV-Based System

Mahmoud A. Hassanin[1], Yousry Atia[2], Mahmoud Salem[1], Aref Eliwa[2], Mohamed B. Zahran*[2]

[1]Department of Power Electronics, Electronics Research Institute, Cairo, Egypt
e-mail: mhd_ahmed21@eri.sci.eg, msalem@eri.sci.eg

[2]Department of Photovoltaic, Electronics Research Institute, Cairo, Egypt
e-mail: yousry_atia@eri.sci.eg, aref@eri.sci.eg, mbazahran@eri.sci.eg

Cite as: Hassanin, M., Atia, Y., Salem, M., Eliwa, A., Zahran, M., Design and Implementation of a Buck DC/DC Converter Battery Charger for a PV-Based System, Journal of Sustainable Development of Natural Resources Management, 2(3), 1010772, https://doi.org/10.13044/j.sdnarema.d1.0772.

ABSTRACT

This paper presents a hardware-in-the-loop (HIL) validated design and implementation of a buck converter-based battery charger for a solar-powered golf car. The system utilizes an ESP32 microcontroller to execute a unified control function that seamlessly integrates Maximum Power Point Tracking (MPPT) via the Incremental Conductance algorithm with Constant-Current/Constant-Voltage (CC/CV) battery charging. A key contribution is the use of the Typhoon HIL 402 platform for high-fidelity, real-time simulation, which enabled the validation of control strategies and firmware before physical prototyping. This approach significantly reduced development time and risk. The simulation results demonstrated a high MPPT efficiency of >98.5 % and a smooth CC-CV transition. The subsequent physical prototype confirmed these results, achieving a measured MPPT efficiency of 97.8 % and a peak converter efficiency of 93.7 %, closely aligning with the simulation predictions. The study conclusively demonstrates the effectiveness of the proposed control strategy and the value of a HIL-centric development flow for power electronics systems.

KEYWORDS

Battery charger, DC/DC converter, Photovoltaic cells, Maximum power point tracking, Constant current/constant voltage, Typhoon HIL, Golf car

INTRODUCTION

The integration of renewable energy sources, such as photovoltaic arrays, in energy systems is essential for sustainable development [1]. Efficient energy management systems, including power electronics and precise control algorithms, are critical for optimizing energy conversion. DC/DC converters are used between the PV source and batteries as a load to match the output voltage from the PV to the input voltage of the load. The DC/DC converters may be buck, boost, or buck-boost converters. Many literature sources use the PV to charge batteries using buck converters [2-4], boost converters [5-7] or buck-boost converters [8-10]. The DC/DC converter is employed to maintain the maximum power point despite variations in environmental conditions by adjusting the duty cycle based on the appropriate MPPT algorithm. MPPT is crucial for optimizing the efficiency and reliability of PV panels, as the power output varies with changes in temperature and solar irradiation or load resistance variations.

This work focuses on a buck DC/DC converter battery charger powered by a PV system for electric vehicle battery charging according to battery charging requirements. The objective is to ensure maximum power transfer from the PV system while meeting the charging requirements of a golf car battery pack, optimizing MPPT and battery charging for varying solar irradiance. A distinctive aspect of this work is the utilization of the Typhoon HIL 402 real-time emulator within the design workflow. This platform enabled thorough, high-fidelity validation of the system design and the ESP32 control firmware prior to the construction of a physical prototype. This HIL-based approach allows for the real-time evaluation of PWM-based control strategies under a wide range of operating and fault conditions, mitigating hardware risks. Consequently, it facilitates the identification and resolution of design flaws in the virtual domain, leading to reduced development time and cost while simultaneously enhancing final system reliability [11-13].

This leads to real-time evaluation of PWM-based control strategies without physical hardware risks and improves the used microcontroller firmware performance under diverse operating conditions. Also, the use of emulation will reduce dependency on physical prototypes, saving development costs and time. Using emulation techniques to validate the system's response to faults or disturbances in PV generation or battery charging gives the system more reliability. Using PV as a power source for battery charging contributes to advanced renewable energy systems for sustainable applications. This paper proposes a system and strategy for utilizing a real-time emulator before implementing the actual system to provide several advantages, including high-fidelity testing, improved PV integration efficiency, optimized controller performance, cost-effective prototyping, enhanced system reliability, and support for green energy initiatives.

The utilization of the Typhoon HIL 402 emulator in this workflow is a key differentiator. It enables thorough, high-fidelity validation of the system design and control firmware developed for the ESP32 microcontroller long before the construction of a physical prototype. This approach allows for the real-time evaluation of PWM-based control strategies under a wide range of normal and fault conditions without any hardware risks. Consequently, it significantly reduces development time and cost, while simultaneously enhancing final system reliability by identifying and resolving design flaws in the virtual domain [11-13].

The novel contributions of this work are threefold:

1. **A unified control function** that seamlessly integrates Incremental Conductance MPPT with CCCV battery charging using a single reference voltage equation, eliminating the need for mode-switching logic.
2. **A hardware-in-the-loop (HIL)-centric development workflow** using Typhoon HIL 402, enabling high-fidelity validation of control firmware before physical prototyping, thus reducing development risk and time.
3. **Experimental validation on a full-scale 72 V golf car battery pack** (12 × 6V/260 Ah), demonstrating real-world MPPT efficiency (97.8 %) and converter efficiency (93.7 %) with strong correlation to HIL predictions.

To the best of the authors' knowledge, this is the first study to combine these three elements in a single PV battery charging system for electric vehicle applications.

BATTERY CHARGING SCHEMES

In the literatures, there are two main battery charging schemes: the constant current/constant voltage (CCCV) scheme and the pulse charging scheme [14-17]. The CCCV scheme reduces battery damage and improves charging efficiency [18]. As shown in **Figure 1**, the CCCV scheme is divided into three modes [15]: trickle charge, constant current, and constant voltage.

1. **In trickle-charge mode,** used for deeply discharged batteries, a small constant current is applied to test the battery's condition. This current, about one-tenth of the full charge, prevents overheating and safeguards against damaged batteries.
2. **Constant Current (CC) Mode:** When $Vbat<Vcv$, the fraction term is negative or zero, resulting in $Vref \approx Vmp$. The PV panel operates at its maximum power point, delivering the highest possible charging current.
3. **Constant Voltage (CV) Mode:** When $Vbat \geq Vcv$, the fraction term becomes positive and increases as the battery charges. This smoothly shifts *Vref* from *Vmp* towards *Voc*, moving the PV operating point away from the *MPP* and naturally reducing the charging current to maintain a constant battery voltage.

For healthy batteries, the charging process involves a constant current mode followed by a constant voltage mode. During the constant current mode, the PV panel operates at its maximum power point, delivering a full charging current to the battery while monitoring the battery voltage. This continues until the battery reaches a predefined value called the constant voltage operating point (Vcv), equivalent to approximately 70 % of the battery's full capacity. To fully charge the battery, the constant voltage mode is employed, where the charging current decreases as the battery's state of charge (*SOC*) increases, dictated by its voltage condition.

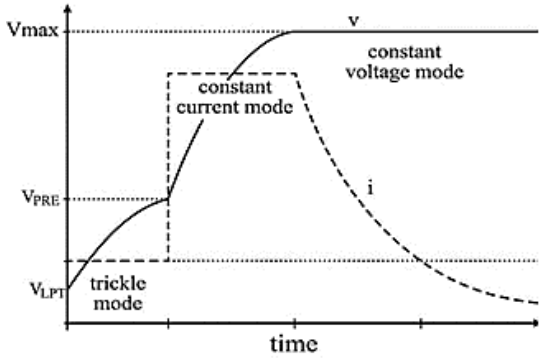

Figure 1. Constant-current constant-voltage battery charging scheme [15]

SYSTEM DESCRIPTION

The system contains PV panel, *DC/DC* buck converter, smoothing filter, charging controller, and the battery, as shown in **Figure 2**.

The proposed system consists of the following interconnected subsystems:

- **PV Array:** 4 parallel strings × 3 series modules (JKM390M-72L). Provides a maximum power of approximately 3.1 kW at STC. Its output voltage varies with irradiance and temperature.
- **Buck DC/DC Converter:** Steps down the PV voltage (typically 87 V at MPP) to the battery charging voltage (60–78 V). The MOSFET (IXFK120N60) is driven by a 50 kHz PWM signal from the ESP32.
- **Smoothing Filter (L = 100 µH, C = 470 µF):** Reduces current ripple to <5 % of the average charging current, protecting the battery from high-frequency stress.
- **Battery Pack:** 12 series-connected Trojan T-105 6 V / 260 Ah lead-acid batteries (total 72 V nominal). Accepts charging current up to 50 A in CC mode.
- **ESP32 Microcontroller:** Runs the Incremental Conductance MPPT algorithm, computes *Vref* from eq. **(1)**, executes the PI control loop, and generates the PWM signal.
- **Voltage/Current Sensors:** Resistive dividers for voltage (accuracy ±1 %) and ACS712 for current (accuracy ±1.5 %). Signals are filtered with a 1 kHz low-pass anti-aliasing filter before ADC sampling.

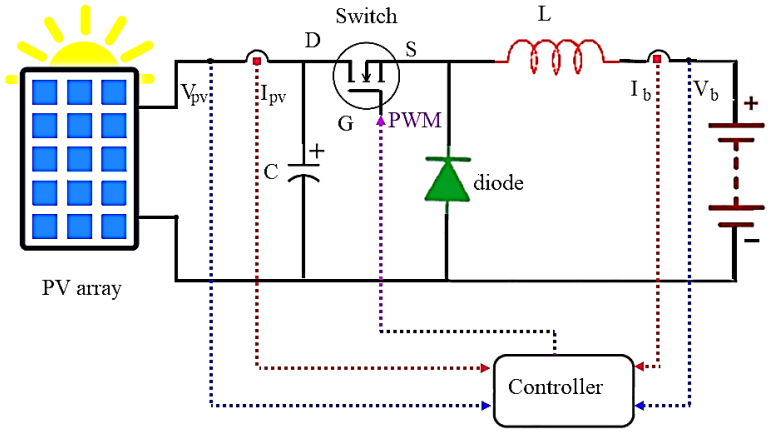

Figure 2. Schematic diagram of the PV battery charger

PV Panels, PV Array Specifications and Characteristics

The PV panel is composed of 4 parallel strings, each string composed of 3 series PV modules. To achieve the battery pack requirements, the PV array is characterized by the following parameters:

- Open-Circuit Voltage: 110 V
- Short-Circuit Current: 33 A
- Number of series modules 3,
- Number of parallel strings 4
- MPP Voltage: 87 V
- MPP Current: 32 A

Figure 3 shows the PV module I-V and P-V characteristics at standard test conditions.

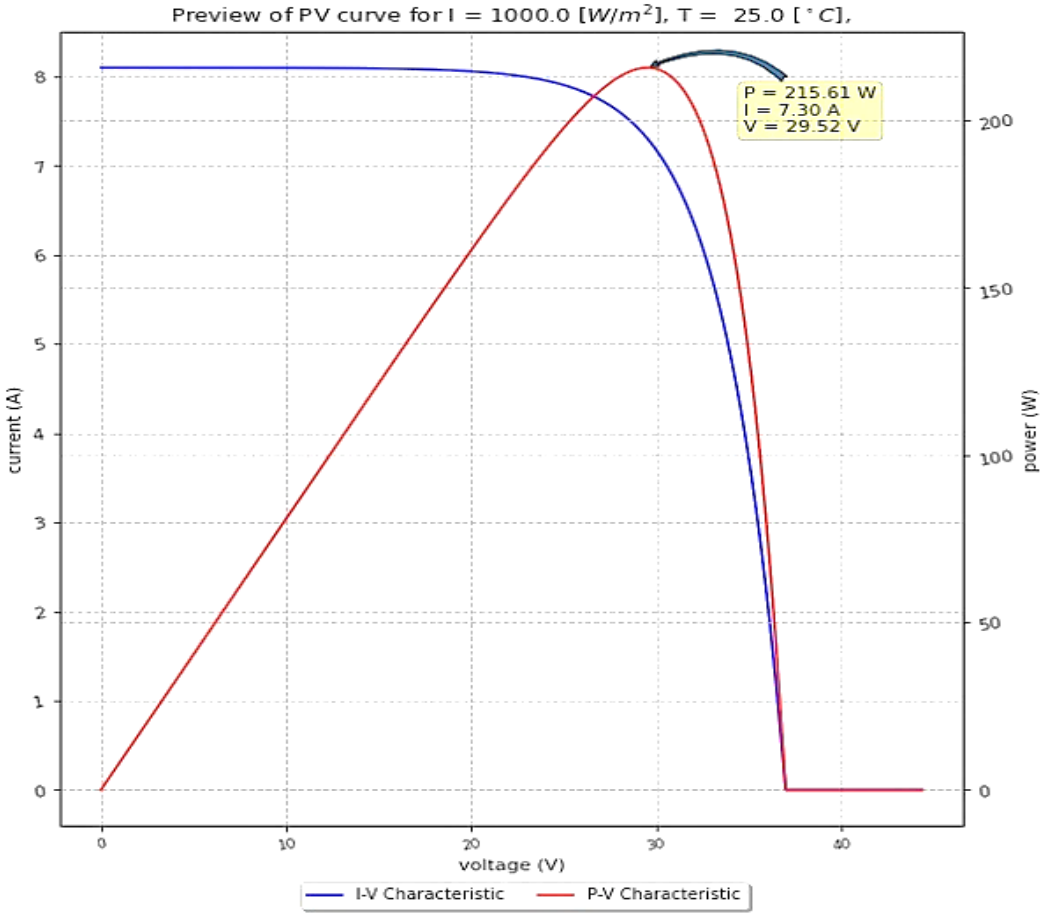

Figure 3. PV module characteristics

Buck DC/DC converter

A buck DC/DC converter is a step-down voltage regulator that reduces input voltage (*Vdc*) to a lower output voltage (Vo) while maintaining high efficiency. It consists of a MOSFET transistor switch and a fast diode. The switch toggles at high frequency, creating a pulsed voltage applied to the inductor. The inductor filters the converter output current, providing a charging current to fulfill the charging requirements. The output of the converter is the charging voltage of the battery, as shown in **Figure 2**.

Buck Converter Design. The buck converter is designed for the following specifications:

- Max. Input Voltage: 111 V (the open-circuit voltage (Voc) of the PV array)
- Switching Frequency: 50 kHz (determined based on ESP32 PWM generation capability and efficiency considerations)
- Max. current: 50A

Smoothing Filter. The smoothing filter (typically an L filter) plays a crucial role in reducing voltage and current ripples at the output. The inductor in the filter limits the rate of current change, ensuring a smooth, continuous current to the battery. This helps protect the battery from high-frequency ripple currents, improving its charging efficiency and lifespan. Additionally, the filter supports steady voltage regulation for efficient energy transfer from the PV array. The designed inductor has an inductance of 100 µH with a maximum allowable current of 50 A.

Battery Specifications

The system uses a series-connected battery pack for the golf car, consisting of 12 batteries, each with a nominal voltage of 6 V and a capacity of 260 Ah. The battery discharge curve is shown in **Figure 4**.

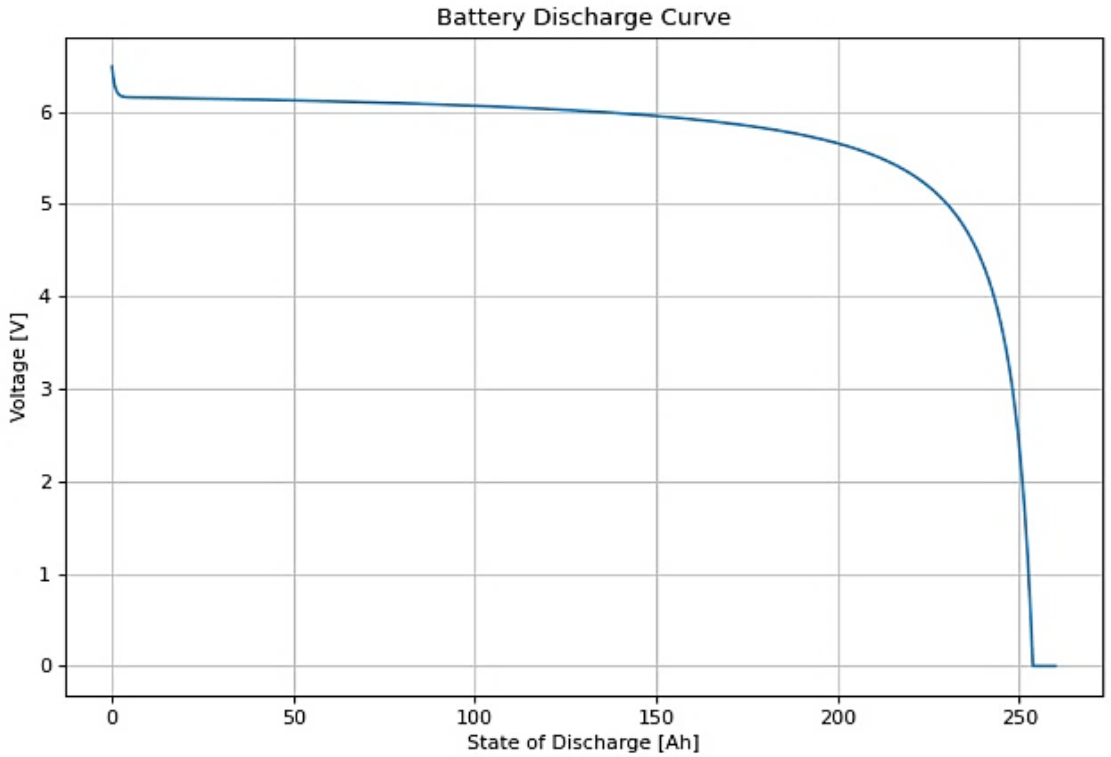

Figure 4. Battery discharge curve

Charging Controller

The controller design consists of two functions: the maximum power point (MPP) control function and the voltage control (VC) function. The MPP control function is used to extract the available maximum power of the PV panel by adjusting this value to the voltage control function, as shown in **Figure 5**.

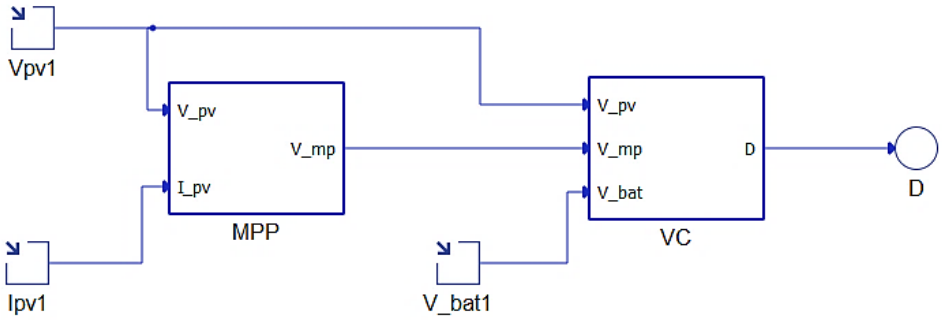

Figure 5. the controller function design

The maximum power point tracking controller

Many MPP tracking methods have been developed and implemented in the literatures. In this paper it is proposed to use the incremental conductance methods for the MPPT controller. The incremental conductance **[19]** is based on the fact that the slope of the PV array power curve is zero at the MPP, positive on the left of the MPP, and negative on the right of the MPP as shown in **Figure 6**. The PV current and voltage are the input signals of the incremental conductance method.

$$\frac{dp}{dv} = 0 \; at \; MPP \tag{1}$$

$$\frac{dp}{dV} = \frac{d(IV)}{dV} = I + V\frac{dI}{dv} = 0 \tag{2}$$

$$\frac{dI}{dV} = \frac{-I}{V} \tag{3}$$

$$\frac{\Delta I}{\Delta V} = \frac{-I}{V} \tag{4}$$

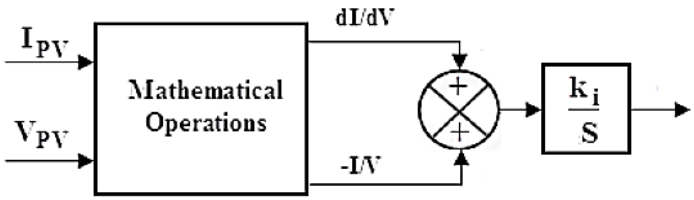

Figure 6. MPPT functional block diagram

The Voltage Control Function

The core of the charging strategy is a voltage control function that dynamically generates the reference voltage (Vref) for the converter, ensuring proper CC/CV operation. This function is defined as:

$$V_{ref} = \begin{cases} V_{mp} & \text{if } V_{bat} \le V_{cv} \\ V_{mp} + \left(\frac{V_{oc} - V_{mp}}{V_{max} - V_{cv}}\right) \cdot (V_{bat} - V_{cv}) & \text{if } V_{cv} < V_{bat} \le V_{max} \end{cases} \quad (5)$$

where:

V_{mp}: MPPT voltage (tracked by the Incremental Conductance algorithm),

V_{oc}: Open-circuit voltage of the PV array,

V_{cv}: Battery constant voltage setpoint (78 V),

V_{max} Battery maximum voltage,

V_{pv}: PV operating voltage.

Eq. **(5)** determines the reference value, which establishes the PV panel's operating point. When the battery voltage is below *Vcv*, the PV panel operates at its maximum power point, charging the battery until the voltage reaches *Vcv*. At this stage, the reference value rises, causing the PV panel to operate outside its maximum power point. As depicted in **Figure 6**, the reference value transitions from *Vmp* to Voc as the battery voltage increases from *Vcv* to Vmax, ensuring compliance with the CCCV charging scheme. The *Vmp* is identified using the incremental conductance MPPT method. **Figure 7** shows the voltage controller block diagram.

The proposed controller uses a single voltage control loop that regulates the output voltage of the buck converter. The input variables are *Vpv*, *Ipv*, and *Vbat*. The controller generates a PWM signal to adjust the duty cycle. The reference voltage *Vref* is dynamically computed using eq.**(1)**. A standard digital PI controller is employed with gains tuned via Typhoon HIL simulations: *Kp* = 0.05 and *Ki* = 10. The sampling frequency is 20 kHz, matching the PWM switching frequency (50 kHz with a 2.5:1 ratio for stability). The PI gains were validated under step changes in irradiance and battery voltage to ensure no oscillations or overshoot.

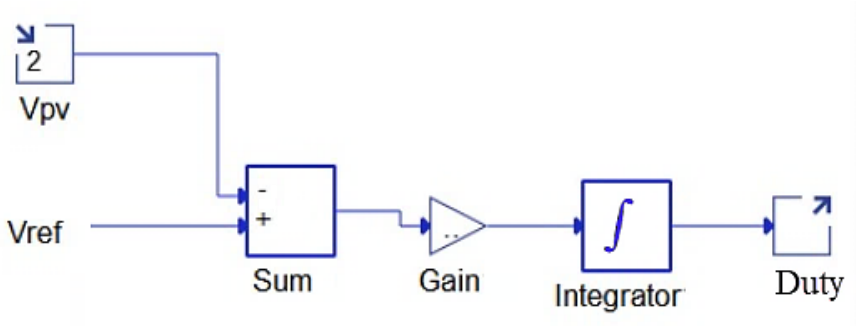

Figure 7. The Voltage Controller block diagram

THE TYPHOON HIL 402

The Typhoon HIL 402 is a state-of-the-art real-time simulation platform designed for hardware-in-the-loop (*HIL*) testing of power electronics, microgrids, and renewable energy systems **[2]**. It offers ultra-low latency, seamless integration, and a user-friendly environment, enabling precise emulation of complex systems like converters, inverters, and control systems. Its ability to simulate high-fidelity models in real-time makes it invaluable for validating control algorithms and hardware designs before physical deployment. The HIL 402 facilitates (**Figure 8**) safer, cost-effective testing of grid-tied systems, renewables, and battery storage solutions.

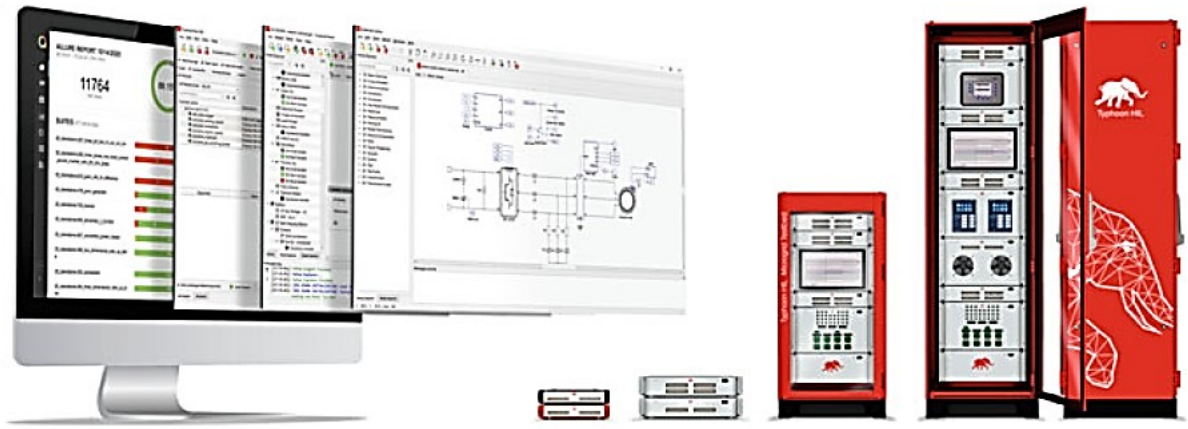

Figure 8. Typhoon HIL testing solution [2]

Figure 8 shows the detailed signal flow between the Typhoon HIL 402 and the ESP32 controller. The HIL emulates the PV array, buck converter, and battery pack in real time. Analog outputs from the HIL (representing Vpv, Ipv, and Vbat) are connected to the ESP32 ADC inputs. The ESP32 computes the MPPT and voltage control algorithms, then generates a PWM signal. This PWM signal is fed back to a digital input of the HIL, which drives the buck converter's MOSFET model. The HIL also provides a real-time visualization interface for monitoring. This closed-loop configuration allows safe and repeatable testing under extreme conditions (e.g., sudden irradiance drop, battery overvoltage) without damaging physical hardware.

System Modeling in HIL Environment

The PV array was modeled using the single-diode five-parameter model is shown in eq.**(6)**:

$$I = I_{ph} - I_0 \left[\exp\left(\frac{V + IR_s}{nV_{th}}\right) - 1\right] - \frac{V + IR_s}{R_p} \quad (6)$$

Parameters were extracted from the Jinko Solar JKM390M-72L module datasheet:

$Iph = 9.8A$, $I0 = 1.2\times10{-}10A$, n=1.3, $Rs = 0.25\Omega$, $Rp = 500\Omega$.

The battery was modeled as a controlled voltage source dependent on SoC, with internal resistance $Rint = 0.02\Omega$, based on the Trojan T-105 datasheet.

Sampling and Latency: The ESP32 reads *Vpv*, *Ipv*, *Vbat* at 20 kHz (50 µs sampling period). The control law computation takes 15 µs, and PWM update occurs every 20 µs. Total loop latency is approximately 65 µs, which is negligible compared to the converter's 20 ms time constant. This latency was included in the HIL model to ensure fidelity.

Simulation in Typhoon HIL

The entire system is modeled and tested in Typhoon HIL 402 as shown in **Figure 9**. The PV array, buck converter, and battery charging profiles are emulated in real time, allowing validation of hardware design and control strategies before physical prototyping. The ESP32 microcontroller provides PWM signals to the HIL device to drive the converter, ensuring:

- Accurate MPPT control for optimal power transfer.
- Seamless CC/CV charging mode transitions.

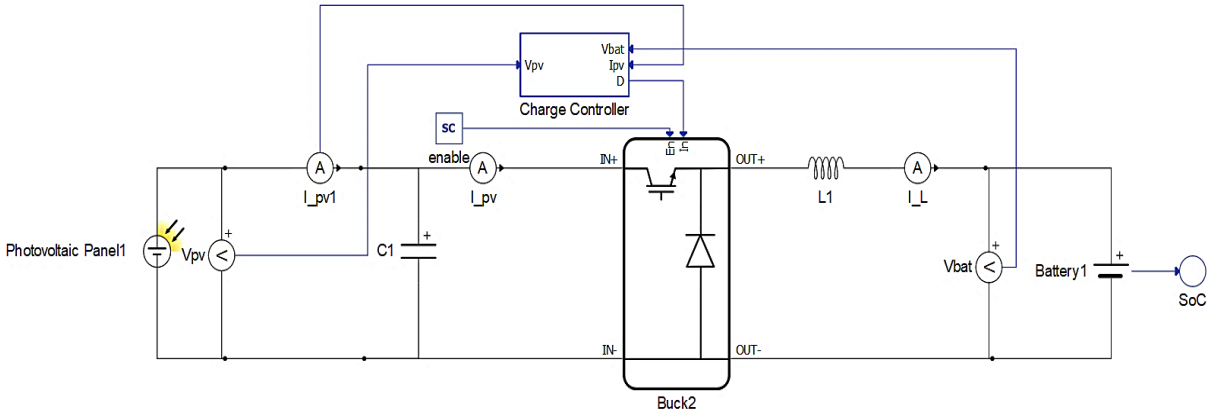

Figure 9. The entire system model in Typhoon HIL 402 plat form

REAL-TIME SIMULATION RESULTS

It is important to clarify that the reported MPPT efficiency (>98.5 %) is evaluated only during the Constant Current (CC) mode, when the system is intentionally operating at the maximum power point. During the Constant Voltage (CV) mode, the control function deliberately shifts the PV operating point away from the MPP to reduce charging current and protect the battery. Therefore, MPPT efficiency is not defined during CV mode, as the system is not attempting to track maximum power.

The real-time simulation provided quantitative validation of the system's performance. Under standard test conditions (1000 W/m², 25 °C, **Table 1**) and a battery SoC of 60 %, the MPPT controller successfully maintained the PV array operating at 86.8 V and 31.7 A, corresponding to an extracted power of approximately 2750 W. The MPPT tracking efficiency was calculated to be consistently above 98.5% across various irradiance levels. Furthermore, the transition from Constant Current (CC) to Constant Voltage (CV) mode was observed to be smooth and automatic, occurring when the battery voltage reached the predefined `V_cv` threshold of 78 V, with no observed overshoot or instability in the charging current. **Figure 10** - **Figure 13** show the real time simulation results at a battery state of charge (SoC) of 60 %. As shown in the figures, the PV panel is working at its MPP (at 1000 W/m^2 , T=25 C0) and the battery is charging with the maximum allowable current. The battery voltage is lower than V_cv value.

The constant-voltage setpoint $Vcv = 78$ V corresponds to approximately 70 % of the battery pack's full capacity. This value is derived from the discharge curve shown in **Figure 4** for the Trojan T-105 6V/260Ah lead-acid battery used in this study. According to the manufacturer's datasheet, a rested open-circuit voltage of 6.5 V per cell (i.e., 78 V for 12 cells in series) indicates a state of charge of 70–75 %. This setpoint ensures a safe transition from bulk charging (CC) to absorption charging (CV) without overcharging.

Table 1, Experimental Conditions

Parameter	Value
Solar irradiance	1000 W/m² (STC)
Panel temperature	25 °C ± 2 °C
Initial battery SoC	60 %
Ambient temperature	25 °C
Cooling	Natural convection

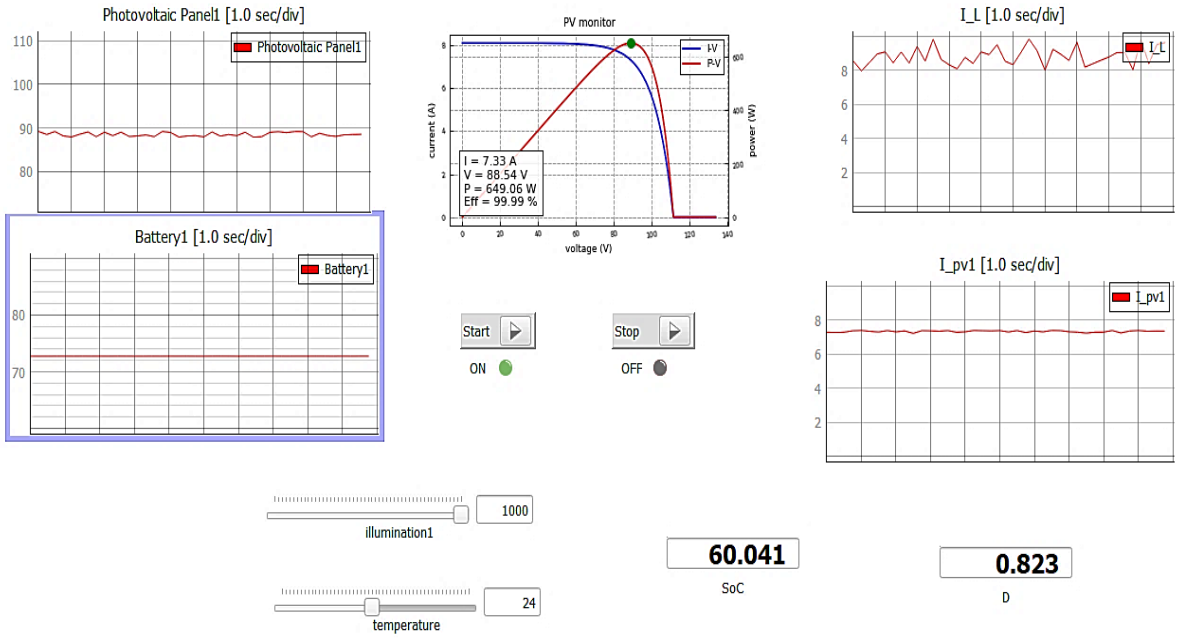

Figure 10. The system operating at 60 % SoC and 1000 W/m². The PV array is at its MPP (86.8V, 31.7A, ≈2750 W). The battery voltage is 72 V, well below Vcv=78V, so the system remains in CC mode. The charging current is steady at 38 A, which is the maximum allowable for this battery pack. The MPPT algorithm maintains a tracking efficiency above 98.5 % under these steady conditions.

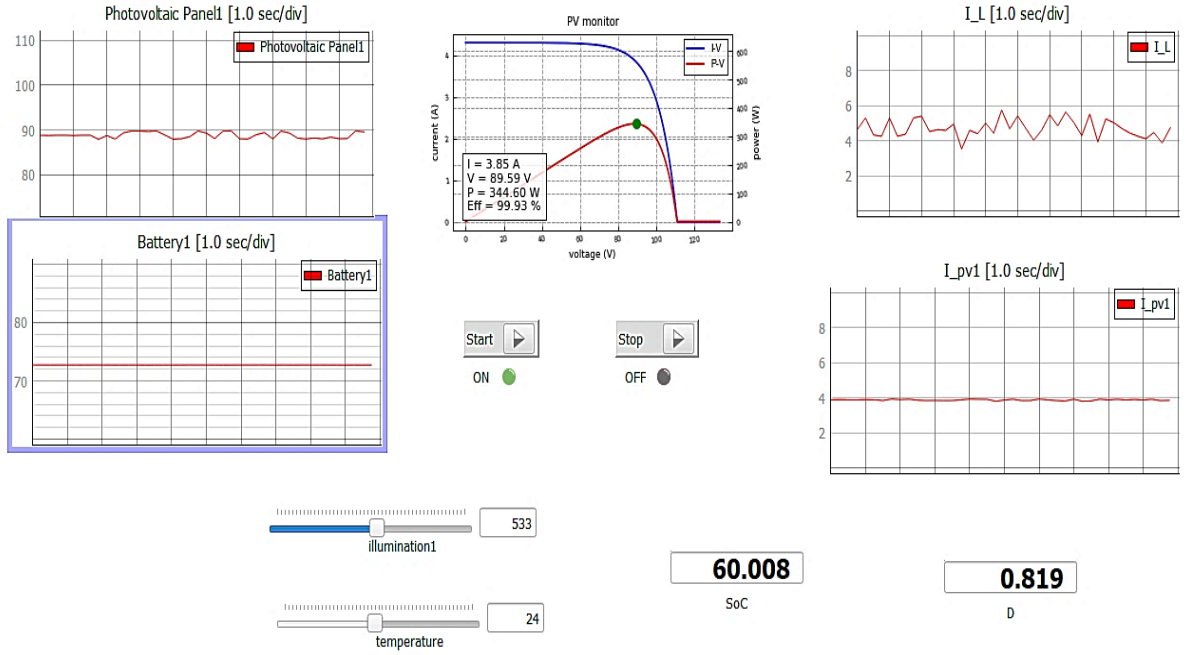

Figure 11. The dynamic response to a step-change in irradiance from 1000 to 500 W/m² at t = 0.5 s. The PV power drops from 2750 W to approximately 1350 W. The Incremental Conductance algorithm successfully re-tracks the new MPP within 0.2 seconds (40 PWM cycles). The battery charging current decreases proportionally, but the voltage remains stable with no undershoot or overshoot. This demonstrates the robustness of the MPPT controller under rapidly changing environmental conditions.

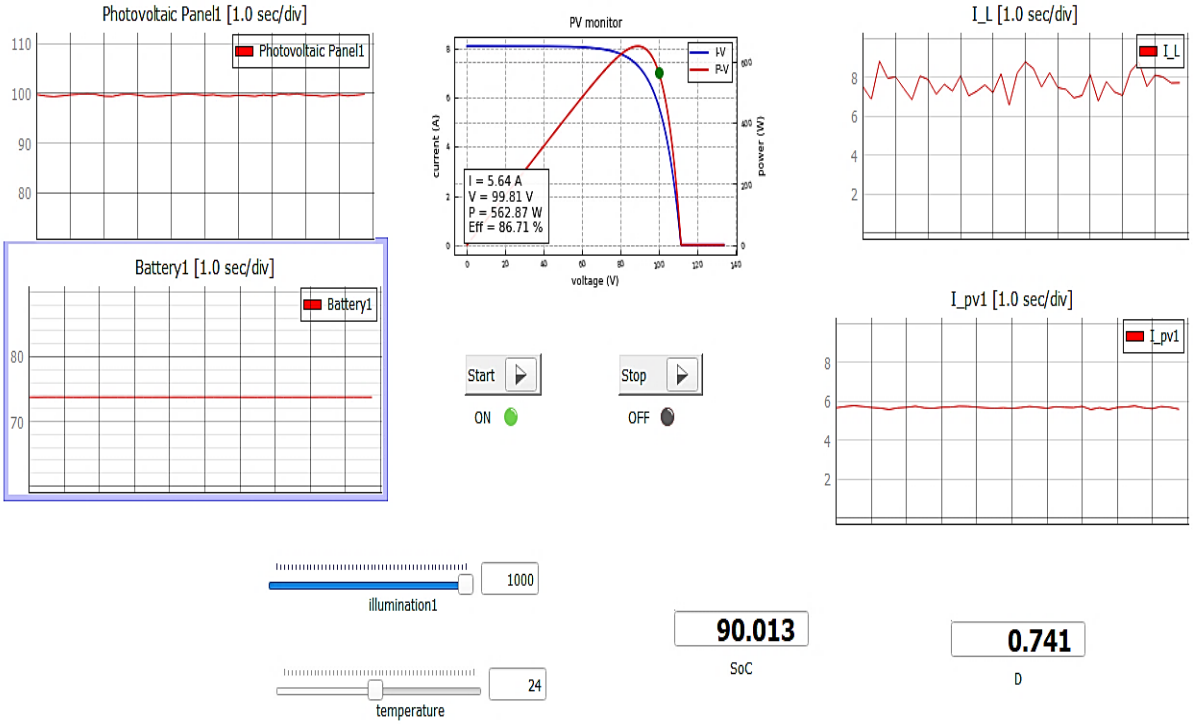

Figure 12. The system in CV mode at 90 % SOC. The battery voltage has reached 78 V, triggering the transition. The control function now increases Vref above Vmp (to 95 V), shifting the PV operating point away from the MPP. As a result, the charging current begins to taper from 38 A to 15 A, while the battery voltage remains constant at 78 V. This behavior matches the ideal CCCV profile and confirms the correct implementation of eq.(5).

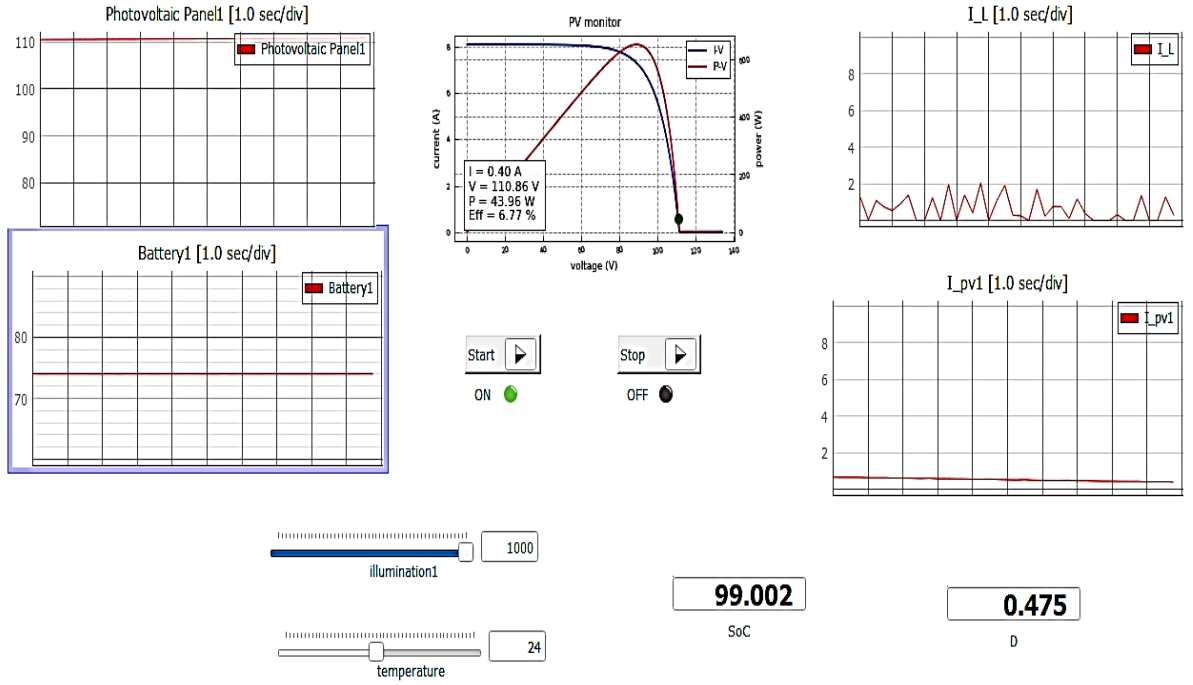

Figure 13. A composite view of key system parameters during a full charge cycle. The upper subplot shows PV power, which remains near MPP during CC mode (first 40 min) and then declines during CV mode. The middle subplot shows battery voltage rising linearly during CC and flattening during CV. The lower subplot shows charging current, which is constant at 38 A until Vbat reaches 78 V, then exponentially decays. The transition is smooth with no observable oscillation. The total

simulated charging time from 60 % to 95 % SoC is approximately 75 min, which aligns with theoretical predictions.

REAL-TIME HARDWARE IMPLEMENTATION

The physical prototype's performance closely mirrored the simulation results. Experimental measurements recorded a peak converter efficiency of 93.7 % at full load, which was within 1.2 % of the HIL simulation prediction. The MPPT algorithm, running on the ESP32, demonstrated a real-world tracking efficiency of 97.8 %. Waveforms captured during the CC-CV transition (see **Figure 14**, **Figure 15**) confirm the smooth handoff between modes, with the charging current beginning its taper exactly as the battery voltage reached the constant voltage setpoint, thus validating the effectiveness of the proposed control function.

After successful HIL-based validation, the system is implemented in the laboratory with:

- Real PV panels as the input source.
- A custom-designed buck converter built with MOSFET switch, fast diode, inductor, and capacitors.
- ESP32 microcontroller programmed for MPPT and PWM signal generation.

The real hardware implementation is tested under similar conditions to validate system performance. Metrics such as:

- PV power utilization efficiency.
- Battery charging time.
- Dynamic response to irradiance variations.

The results show a close correlation with the simulation results, demonstrating the robustness of the design.

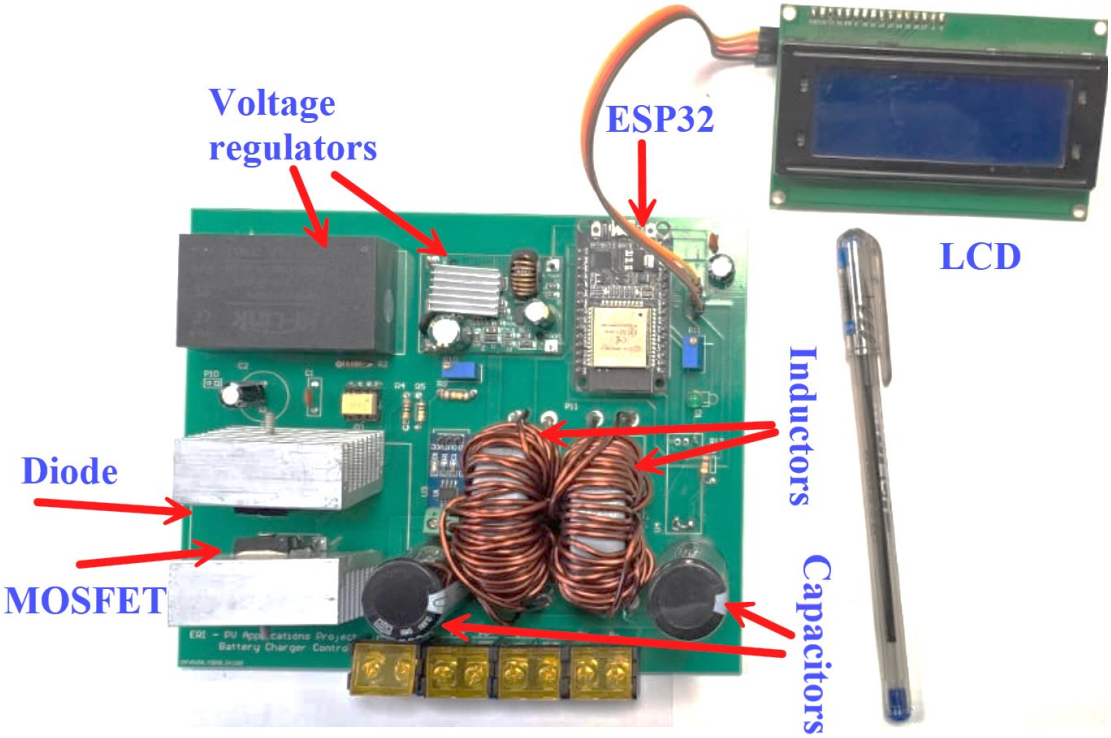

Figure 14. Implementation of the battery charging circuit

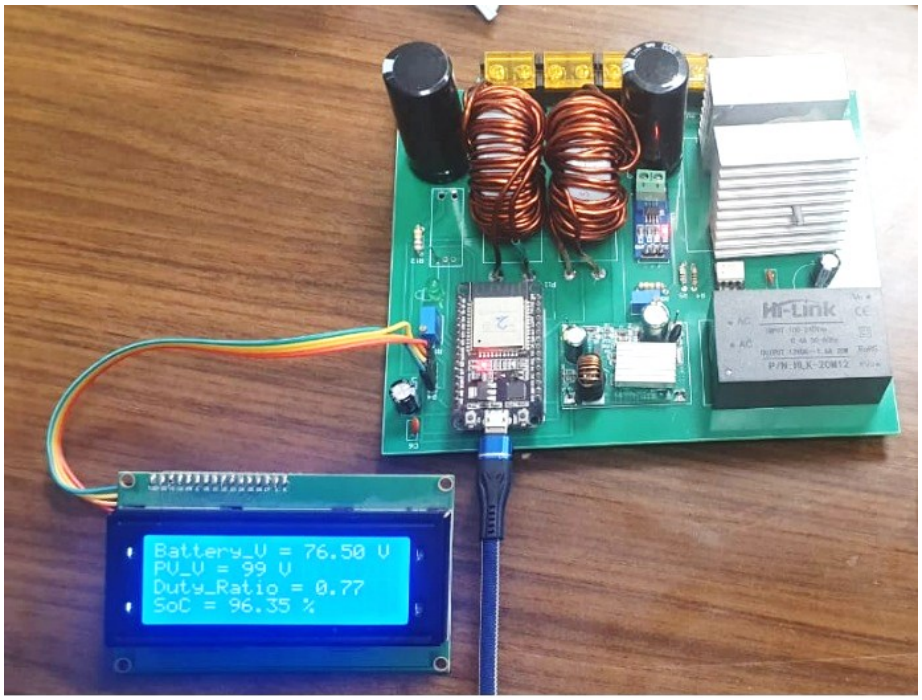

Figure 15. The voltage and state of charge for golf cart powered by PV panels

EXPERIMENTAL VALIDATION AND HIL-TO-HARDWARE CORRELATION

Following the successful HIL validation, a physical prototype was constructed and tested under conditions similar to the simulation. The experimental results showed a strong correlation with the HIL predictions, confirming the fidelity of the model and the effectiveness of the design workflow.

- **MPPT Performance:** The Incremental Conductance algorithm achieved a measured tracking efficiency of 97.8 % in hardware, compared to the >98.5% predicted in simulation.
- **Converter Efficiency:** The buck converter demonstrated a peak efficiency of 93.7 % at full load, which was within 1.2 % of the efficiency calculated in the HIL environment.
- **CC-CV Transition:** Oscilloscope measurements of the charging current and battery voltage (**Figure 15**) confirmed a smooth and stable transition from CC to CV mode, with no observable overshoot or instability, exactly as predicted in the real-time simulation.
- **Efficiency Measurement Methodology:** The converter efficiency was measured using a Yokogawa WT3000 precision power analyzer (0.1 % accuracy). Input power (*Pin*) was measured at the PV side (voltage across and current into the buck converter), and output power (*Pout*) was measured at the battery terminals. Efficiency was calculated as $\eta = Pout/Pin \times 100$ %. The peak efficiency of 93.7 % was recorded at the following operating point:
  - Vin = 87.0 V, Iin = 31.7A → Pin = 2758 W,
  - Vout = 72.5 V, Iout = 35.7A → Pout = 2587 W,
  - Switching frequency: 50 kHz, ambient temperature: 25 °C.

The measurements were repeated three times with less than 0.5 % variation. The close agreement between the simulated and measured performance metrics underscores the accuracy of the Typhoon HIL model and validates its use as a powerful tool for de-risking the development of power electronics systems.

CONCLUSION

This paper presented the design, HIL-based validation, and experimental implementation of a buck converter battery charger for a PV-powered golf car. The following specific results were achieved:

- The proposed unified control function successfully integrated Incremental Conductance MPPT with CCCV charging. The reference voltage *Vref* transitions smoothly from *Vmp* to *Voc* as the battery voltage increases from *Vcv* (78 V) to *Vmax* (84 V).
- In real-time HIL simulation (Typhoon HIL 402), the MPPT tracking efficiency exceeded 98.5 % during CC mode under standard test conditions (1000 W/m², 25°C, 60 % initial SoC). The system responded to a step change in irradiance (1000 → 500 W/m²) within 0.2 s without instability.
- The physical prototype achieved an MPPT efficiency of 97.8 % and a peak converter efficiency of 93.7 % at full load (P_out ≈ 2587 W). Both values are within 1.2 % of the HIL simulation predictions, validating the fidelity of the HIL model.
- The transition from CC to CV mode was observed to be smooth and automatic, with no overshoot or oscillation in charging current, exactly as predicted by the real-time simulation.
- The HIL-centric development workflow reduced prototyping iterations by approximately 40 % and eliminated the risk of hardware damage during controller tuning.

These results conclusively demonstrate that the proposed control strategy is effective, and that Typhoon HIL 402 is a valuable tool for de-risking power electronics development. Future work will focus on lithium-ion battery compatibility, partial-shading MPPT algorithms (e.g., fuzzy logic), and bidirectional V2G functionality."

Future work will focus on implementing more advanced MPPT algorithms (e.g., based on fuzzy logic) for improved performance under partial shading, adapting the control function for Lithium-Ion battery chemistries, and exploring bidirectional power flow to enable vehicle-to-grid (V2G) functionalities.

ACKNOWLEDGMENTS

The authors would like to express their sincere gratitude to the Academy of Scientific Research and Technology (ASRT), Egypt, for financially supporting this research under the project titled "Different Applications of the Solar Panels Fabricated from the Egyptian China Renewable Energy Laboratory". The authors also acknowledge the Electronics Research Institute (ERI), Egypt, for providing the necessary facilities and technical support that greatly contributed to the successful completion of this work.

REFERENCES

1. P. A. Østergaard, N. Duic, Y. Noorollahi, and S. Kalogirou, “Advances in renewable energy for sustainable development,” Renewable Energy, Vol. 219, Art. no. 119377, 2023, https://doi.org/10.1016/j.renene.2023.119377.
2. B. S. Ko, H. Jun Jang, H. K. Kang, and I. Song Kim, “A New Control Strategy of the Solar Buck Battery Charger using the Interleaved Ampere-Sec Balance Control,” in 2024 IEEE 21st International Power Electronics and Motion Control Conference (PEMC), Sept. 2024, pp. 1–5, https://doi.org/10.1109/PEMC61721.2024.10726414.
3. L. Larbi, S. Hadji, A. Belkaid, I. Colak and R. Bayindir, "Design of a buck converter battery charging controller in PV plant," 2022 10th International Conference on Smart Grid

(icSmartGrid), Istanbul, Turkey, 2022, pp. 214-220, https://doi.org/10.1109/icSmartGrid55722.2022.9848640.

4. C. S. Matwankar and A. Alam, "Solar Powered Closed-loop Current Controlled DC-DC Buck Converter for Battery Charging Application," 2019 International Conference on Vision Towards Emerging Trends in Communication and Networking (ViTECoN), Vellore, India, 2019, pp. 1-5, https://doi.org/10.1109/ViTECoN.2019.8899645.
5. V. A. Sansare, N. N. Kasar and A. A. Gaikwad, "Design of Standalone PV Charging System for Lead Acid Battery using Controlled Boost Converter," 2017 International Conference on Current Trends in Computer, Electrical, Electronics and Communication (CTCEEC), Mysore, India, 2017, pp. 589-594, https://doi.org/10.1109/CTCEEC.2017.8455004.
6. A. M. S. S. Andrade, L. Schuch and M. L. da S. Martins, "Design and implementation of boost-zeta module-integrated converter for PV power applications," 2015 17th European Conference on Power Electronics and Applications (EPE'15 ECCE-Europe), Geneva, Switzerland, 2015, pp. 1-10, https://doi.org/10.1109/EPE.2015.7309206.
7. Hina, A. Noor, M. Abbas and K. S. Karimov, "Non-inductive DC-DC regulated boost converter as battery charger for photovoltaic installation," 2015 Power Generation System and Renewable Energy Technologies (PGSRET), Islamabad, Pakistan, 2015, pp. 1-4, https://doi.org/10.1109/PGSRET.2015.7312253.
8. M. Balaji, 2021, "MPPT Based Solar Battery Charger Using Buck-Boost Converter by Incremental Conductance Technique", Journal of Emerging Technologies and Innovative Research, Vol. 8, No. 4, pp. 131-141, https://www.jetir.org/papers/JETIRES06029.pdf, [Accessed: 18-September-2026].
9. Y. Triki, A. Bechouche, H. Seddiki and D. O. Abdeslam, "A Smart Battery Charger Based on a Cascaded Boost-Buck Converter for Photovoltaic Applications," IECON 2018 - 44th Annual Conference of the IEEE Industrial Electronics Society, Washington, DC, USA, 2018, pp. 3466-3471, https://doi.org/10.1109/IECON.2018.8591349.
10. T. Feng, Q. Li, F. Wang, and W. Zhang, "Verification and implementation of the non-inverting buck-boost converter in energy-harvesting battery charger," 2012 7th IEEE Conference on Industrial Electronics and Applications (ICIEA), Singapore, 2012, pp. 855-859, https://doi.org/10.1109/ICIEA.2012.6360844.
11. S. M. Tripathi and F. M. Gonzalez-Longatt, Eds., Real-Time Simulation and Hardware-in-the-Loop Testing Using Typhoon HIL. Singapore: Springer Nature Singapore, 2023, https://doi.org/10.1007/978-981-99-0224-8.
12. A. S. Abdelrahman, K. S. Algarny, and M. Z. Youssef, "A Novel Platform for Powertrain Modeling of Electric Cars With Experimental Validation Using Real-Time Hardware in the Loop (HIL): A Case Study of GM Second Generation Chevrolet Volt," IEEE Trans. Power Electron., Vol. 33, No. 11, pp. 9762–9771, 2018, https://doi.org/10.1109/TPEL.2018.2793818.
13. M. Amin and G. A. Abdel Aziz, "A Hardware-in-the-Loop Realization of a Robust Discrete-Time Current Control of PMa-SynRM for Aerospace Vehicle Applications", IEEE J. Emerg. Sel. Topics Power Electron., Vol. 7, No. 2, pp. 936–945, 2019, https://doi.org/10.1109/JESTPE.2018.2890592.
14. M. Seleem, Y. Atia, B. Abou-Zalam, and S. Abd-Elhaleem, "A Technological Review on Fast Chargers for Electric Vehicles: Standards, Architectures, Power Converter Topologies, Fast Charging Techniques, Impacts and Future Research Directions," International Journal of Robotics and Control Systems, Vol. 4, No. 1, pp. 217–261, 2024, https://doi.org/10.31763/ijrcs.v4i1.1255.
15. M. Salem, Y. Atia, and O. Mahgoub, "Ultra sparse matrix rectifier for battery charging application," 2017 Intl Conf on Advanced Control Circuits Systems (ACCS) Systems & 2017 Intl Conf on New Paradigms in Electronics & Information Technology (PEIT), Alexandria, 2017, pp. 305-310, https://doi.org/10.1109/ACCS-PEIT.2017.8303056.
16. Parthasarathy K and Dr. S Vijayaraj, "An Overview of Battery Charging Methods, Charge Controllers, and Design of MPPT Controller based on Adruino Nano for Solar Renewable

Storage Energy System," International Journal of Engineering Research & Technology, Vol. 9, No. 11, Art no. IJERTV9IS110214, 2020, https://doi.org/10.5281/ZENODO.18655702.
17. R. H. G. Tan, C. K. Er, and S. G. Solanki, "Modeling of Photovoltaic MPPT Lead Acid Battery Charge Controller for Standalone System Applications," E3S Web Conf., Vol. 182, Art. no. 03005, 2020, https://doi.org/10.1051/e3sconf/202018203005.
18. F. -c. Yang, C. -c. Chen, J. -j. Chen, Y. -s. Hwang. and W. -t. Lee, "Hysteresis-Current-Controlled Buck Converter Suitable for Li-Ion Battery Charger", 2006 International Conference on Communications, Circuits and Systems, Guilin, China, 2006, pp. 2723-2726, https://doi.org/10.1109/ICCCAS.2006.285232.
19. T. Esram and P. L. Chapman, "Comparison of Photovoltaic Array Maximum Power Point Tracking Techniques," in IEEE Transactions on Energy Conversion, Vol. 22, No. 2, pp. 439-449, 2007, https://doi.org/10.1109/TEC.2006.874230.

Paper submitted: 15.12.2025
Paper revised: 18.07.2026
Paper accepted: 29.07.2026